



ZnO-In₂O₃-SnO₂ THIN FILM TRANSPARENT HEATERS: TUNABLE ELECTROTHERMAL PROPERTIES THROUGH SUBSTRATE TEMPERATURE AND POSTGROWTH ANNEALING

^{1,3,*}Hasan AKYILDIZ , ²Hilal Aybike CAN , ³Burak KIVRAK , ⁴Tayfur ÖZTÜRK 

^{1,3} Konya Technical University, Engineering and Natural Sciences faculty, Metallurgical and Materials Engineering Department, Konya, TÜRKİYE

^{2,4} Middle East Technical University, Engineering Faculty, Metallurgical and Materials Engineering Department, Ankara, TÜRKİYE

³ Konya Technical University, Nanotechnology and Advanced Materials Development Application and Research Center, Konya, TÜRKİYE

^{1,3} hakyildiz@ktun.edu.tr, ² hilal.can@epfl.ch, ³ bkivrak@ktun.edu.tr, ⁴ ozturk@metu.edu.tr

Highlights

- Amorphous ZnO-In₂O₃-SnO₂ thin film transparent heaters were produced with a specific composition via magnetron sputtering
- The films produced at 150 °C showed exceptional electrothermal response
- The saturation surface temperature was measured as 112 °C
- The areal power density was calculated as 0.4635 Watt/cm² for an applied potential of 12V
- The heater melted all ice and evaporated the residual water droplets within 173 s



ZnO-In₂O₃-SnO₂ THIN FILM TRANSPARENT HEATERS: TUNABLE ELECTROTHERMAL PROPERTIES THROUGH SUBSTRATE TEMPERATURE AND POSTGROWTH ANNEALING

^{1,3,*}Hasan AKYILDIZ^{ID}, ²Hilal Aybike CAN^{ID}, ³Burak KIVRAK^{ID}, ⁴Tayfur ÖZTÜRK^{ID}

^{1,3} Konya Technical University, Engineering and Natural Sciences faculty, Metallurgical and Materials Engineering Department, Konya, TÜRKİYE

^{2,4} Middle East Technical University, Engineering Faculty, Metallurgical and Materials Engineering Department, Ankara, TÜRKİYE

³ Konya Technical University, Nanotechnology and Advanced Materials Development Application and Research Center, Konya, TÜRKİYE

^{1,3}hakyildiz@ktun.edu.tr, ²hilal.can@epfl.ch, ³bkivrak@ktun.edu.tr, ⁴ozturk@metu.edu.tr

(Received: 25.11.2024; Accepted in Revised Form: 16.12.2024)

ABSTRACT: Amorphous thin films of ZnO-In₂O₃-SnO₂ (a-ZITO) were manufactured using magnetron sputtering technique for the applications of thin film transparent heaters (TFTHs). For this purpose, a custom-made 3" sputtering target was prepared with a specific composition in terms of the atomic percentages (at.%) of Zn, In, and Sn cations. The impact of varying substrate temperatures on the characteristics of the samples investigated by depositing the films on glass substrates maintained at room temperature, 150 °C, and 250 °C. To improve the optical and electrical properties, post-growth annealing was carried out under forming gas atmosphere at 400 °C. Structural, morphological, optical, and electrical properties of the samples were thoroughly examined. Electrothermal characterization was performed on samples at room temperature and -40 °C to evaluate response time, saturation temperature, thermal homogeneity, stability, recyclability, thermal resistance, and the defogging/deicing capability of the produced TFTHs. The films produced at 150 °C demonstrated an exceptional electrothermal response, with the thermal resistance calculated to be 181.7 °C·cm²/W under 12 V input. With a measured power density of 0.4635 Watt/cm², this heater was able to melt all ice and evaporate water droplets on the surface within 173 s, indicating a promising performance for commercial defogging/deicing applications.

Keywords: ZnO, In₂O₃, SnO₂, Transparent Heater, Sputtering, Thin Film, Postgrowth Annealing

1. INTRODUCTION

Numerous transparent conductive oxide (TCO) compositions identified within the ternary ZITO system are of significant importance as alternatives to Tin-doped Indium Oxide (ITO) in various optoelectronic applications [1-3]. Over the past two decades, crystalline/amorphous thin films of ZITO have been studied for diverse applications, such as active channel layer in thin film transistor (TFT) and nonvolatile memory applications [4-12], as an anode material in organic light-emitting diodes (OLEDs) [13-17], as transparent electrode in organic photovoltaic devices [18-20], dye-sensitized solar cells [21], and polymer dispersed liquid-crystal smart windows [22, 23], as radiating element for optically transparent antennas [24], and as thermoelectric material in transparent display devices [25].

In parallel with the aforementioned studies, the processing parameters, as well as the structural, morphological, optical, and electrical properties including refractive index, extinction coefficient, Fermi level and work function of ZITO thin films were reviewed [26-33]. In addition, Kim et al., have demonstrated that ZITO thin films with Zn-cation concentration above 8.8 at.% are physically stable against hydrogen plasma [34]. Furthermore, Proffit et al., revealed that the crystallization onset temperature of an a-ZITO thin film strongly depends on the cation composition, and requires higher activation energy for crystallization than amorphous ITO [35]. This makes the ternary composition more suitable for applications requiring an amorphous arrangement. Additionally, thin films of a-ZITO have shown promising performance as transparent electrode material in flexible optoelectronic applications

*Corresponding Author: Hasan AKYILDIZ, hakyildiz@ktun.edu.tr

owing to their high visible transmittance, low sheet resistance, high work function, mechanical durability, and lower processing temperatures compatible with numerous polymeric substrates [36-39]. Besides external inner/outer bending, uniaxial stretching, and twisting test results showed that a-ZITO thin films exhibit better mechanical durability than ITO [40]. Therefore, the material was employed as a transparent conducting layer for WO_3 -based flexible electrochromic devices [41]. This device functioned for about 450 cycles without any reduction in electrochromic performance and displayed wider optical modulation and higher coloration efficiency compared to a device with a glass substrate and ITO conducting layer. In another study, an ultra-flexible organic photovoltaic cell was fabricated as a power source for wearable devices, using a layer of a-ZITO as the transparent electrode [42]. It was reported that 94.8% of the initial value of photo conversion efficiency was retained even after 1000 cycles of compression and relaxation test. Recently, Biswas et al., showed that the bending-induced effects on the optical and electrical properties of ZITO transparent electrode could be reduced substantially by inserting an organic semiconductor layer between the electrode and the active layer, maintaining performance up to 20,000 cycles [43]. These results provide strong evidence for the suitability of a-ZITO compositions in future flexible optoelectronic devices.

At this point it is worth remembering that the ternary system of $\text{ZnO-In}_2\text{O}_3\text{-SnO}_2$ includes various well identified compositions such as $\text{In}_{2-2x}\text{Sn}_x\text{Zn}_x\text{O}_3$ solid solution or layered homologous series compounds of $(\text{ZnO})_k\text{-(In}_2\text{O}_3)_m\text{:Sn}$ [2, 3]. It can be inferred from the literature that the preferred compositions for TFT applications are generally composed of slightly Zn-rich compositions, with In:Zn:Sn atomic ratios of 1:1.25:0.25, 1:1.2:0.5 or 1:4.2:1.5 and In:Zn:Sn:P = 1.1:1:0.1:0.01 at.% [5, 6, 9-11]. In contrast, In-rich thin films (~55 to 74 at.% In) have been widely studied for OLED applications [14-17]. For flexible optoelectronic devices, ZITO transparent electrodes were produced from ceramic targets consisting of 70-80 at. % In_2O_3 [39, 41, 42], while the compositions ranging from 30 to 60 at.% In have been investigated for organic photovoltaics [18-20]. The use of varied compositions for different applications is expected due to the unique requirements of each application. It is well documented that the structural, optical, and electrical properties of ZITO strongly depends on the corresponding cations (i.e., In, Zn, and Sn) ratio and as well as to the oxygen content [14, 15, 20, 25, 28-31, 35]. In fact, this compositional flexibility is advantageous for manipulating the properties of the ZITO thin films for specific applications. On the other hand, for thin film production methods such as in sputtering, one must prepare numerous different targets having different compositions to achieve or determine the thin film with the best atomic ratio that is suitable for any particular application. Thus, research on techniques that is expected to allow reduction in necessary time and sintering temperature as well as In-loss during the target preparation is continue [44, 45]. But the improvements in the synthesis of those ceramic targets do not directly solve the problem related to the identification of the perfect film composition for any specific application. Therefore, the combinatorial method may be considered as the best, fastest, and low-cost approach to establish any potential composition in this ternary system by constructing a thin film library with compositional gradient within a few deposition experiments [46, 47]. Following this approach, compositionally gradient ZITO thin films were produced by co-sputtering of high purity individual In_2O_3 , ZnO, and SnO_2 targets [48, 49]. The effects of sputtering pressure, deposition time, substrate temperature, and various post-growth annealing atmospheres on the morphological, structural, optical, and electrical properties were examined in detail. As a result of these studies, a few potential crystalline/amorphous film compositions have been determined with optimal electrical and optical properties for different optoelectronic applications. However, we have identified that there is no study in literature showing the transparent thin film heater properties of ZITO thin films.

In this paper, one of those potential compositions (i.e., 49.6 at.% Zn, 44.5 at.% In, and 5.9 at.% Sn) was selected as the base composition for a 3" sputtering target. ZITO-TFTHs with 37.5 cm² area were deposited onto the glass substrates at three different substrate temperatures using magnetron sputtering. The visual, structural, morphological, optical, electrical, and electrothermal properties of these transparent heaters were examined and compared in both their as-deposited and annealed states. The study has shown that ZITO thin films are good candidates for replacing the commercially available TFTHs, offering significantly

lower In content than ITO and providing sufficiently high-power density for moderate size deicing applications.

2. EXPERIMENTAL

2.1 Thin Film Production

To achieve a single composition ZITO thin films, initially a 3" sputtering target was prepared with In:Zn:Sn cation at.% of 44.5:49.6:5.9. For this purpose, ZnO (45 μm, 99.999%, Sigma Aldrich), In₂O₃ (45 μm, 99.99%, Nanografi), and SnO₂ (45 μm, 99.9%, Nanografi) powders were mixed, compacted and then sintered. The details of the method can be found elsewhere [50]. Prior to deposition, all substrates were cleaned using a sonication bath and hot alkaline detergent, acetone, and absolute alcohol mediums. The 3" sputtering target was located 15 cm away from a circular substrate holder (Ø=15 cm) carrying up to two 1.5 mm thick and 37.5 cm² microscope slide glass substrates. The base pressure was adjusted to 1x10⁻⁶ Torr. The sputtering gas (99.999% Ar) pressure was set to 3 mTorr using a flow rate of 20 Sccm. After a 10 min of pre-sputtering under closed-shutter configuration, ZITO thin films were deposited on the glass substrates maintained at RT, 150 °C or 250 °C. The radio frequency sputtering power was fixed to a constant value of 100 W. During the deposition process, the substrate holder was rotated at 30 rpm and the film thicknesses were limited to 750 nm using a quartz crystal micro balance thickness monitor. For various characterization techniques, thin films on 18 mm diameter glass substrates were also produced using identical deposition parameters.

Once the samples cooled to room temperature under vacuum, films were transferred to an atmosphere-controlled furnace for post-growth annealing. The films were heated to 400 °C at a rate of 2 °C/min in a flowing Ar + 4% H₂ atmosphere and held at this temperature for 90 min. Subsequently, the samples were furnace-cooled ensuring the forming gas environment remained undisturbed.

2.2 Characterization

The crystalline/amorphous states of as-deposited and annealed films were identified using X-ray diffraction (XRD) method via a Bruker D8 Advance diffractometer equipped with a Cu X-ray tube (λ=1.5406 Å). The patterns were obtained in Bragg-Brentano mode with a step-size of 0.02° in the range of 2θ = 20-80°. Morphological and topographical examinations were carried out on both surface and cross-sectional areas of the films using FEI Nova NanoSem 430 model field emission scanning electron microscope (FE-SEM) and Veeco Multi-Mode V model atomic force microscope (AFM), operating in non-contact mode for the construction of 3D surface topography of ZITO thin films. Surface roughness values were determined from the scans over a 2 μm x 2 μm area. The atomic ratios of the cations in the prepared samples were estimated using Energy-dispersive X-ray spectroscopy (EDX). Additionally, a VWR 3100-PC model UV-Vis (ultraviolet-visible) spectrophotometer was employed to measure visible transmittance of ZITO thin films. Spectra were recorded in the wavelength ranges between 350-900 nm, however the data was evaluated between 400 to 700 nm for the calculation of average visible light transmittance (T_{vis}) of the samples. Band gap values were estimated using $(\alpha hv)^2 = A(hv - E_g)^{1/2}$ equation and Tauc plots. In the equation, the terms α , hv , and A stand for absorption coefficient, photon energy, and a constant, respectively. The optical bandgap energy (E_g) was extracted from $(\alpha hv)^2$ vs hv plots by intersecting the extrapolated linear region of the $(\alpha hv)^2$ to the energy axis. Hall-effect measurements (Nanomagnetic Instruments, ezHEMS model) were carried out to determine the electrical properties. For this purpose, thin films were reproduced under identical deposition conditions on 18 mm diameter glass substrates. The measurements were performed on these samples. I-V measurements were conducted at room temperature on as-deposited and annealed thin films using the Van der Pauw configuration and 10 mA current. Measurements were repeated three times. To calculate the Figure of merit (FOM) values, Haacke

equation ($\varphi_{TC} = T_{550\text{ nm}}^{10}/R_s$) was used. In this equation, T_{550} refers to the transmittance at 550 nm wavelength, and R_s (Ω/\square) is the sheet resistance of the ZITO thin film sample.

Electrothermal behavior of ZITO thin films were characterized using a custom-made measurement set up described in detail elsewhere [51]. Briefly, this setup includes a DC power supply (Tektronix PWS4602), an infrared camera (Optris Xi 400), a computer for image processing and a sample holder. The images were recorded at 55 cm distance from the film surfaces. ZITO TFTHs were subjected to constant DC voltages (i.e., 3, 6, 9, and 12 V) at RT to determine the response time, saturation temperature, temperature homogeneity and stability, recyclability, and thermal resistance of the samples. To assess the defogging/deicing capability, the heaters were first placed in a thermally insulated box cooled with dry-ice for 1 h. A humidifier was used to supply the vapor to the environment, creating conditions for ice condensation on the surface. After the sample was removed from the box, the power supply was turned on at 6, 9 or 12 V when the infrared camera indicated a mean surface temperature of -40 °C. The increase in the surface temperature was recorded for each test using the camera. The deicing time was defined as the total duration elapsed for melting and subsequent evaporation of water droplets from the surface. The electrical connection between the power source and the film is provided by duck mouth Cu crocodile clips and Ag electrodes applied to the film surface.

The spatial distribution or the homogeneity of the surface temperature was calculated using the equation $T_U = [(T_H - T_L)/2T_{avg}] \times 100$. T_H , T_L , and T_{avg} refer to highest, lowest and average temperatures recorded from the surface of the sample during the stability test, respectively. The highest and lowest temperatures were determined using an area of $1\text{ mm} \times 1\text{ mm}$, whereas the entire active area was used to compute the average value.

The areal power density of the TFTHs was determined by using the basic electrical formula P/A . Here, P refers to electrical power ($P=I^2R$) and A denotes to the total heater area between the Ag-electrodes. While the current (I) passing through the film is monitored from the power supply, the resistance (R) was calculated by solving the $R=\rho(L/W_e d_k)$ equation. In this equation, ρ (Ωcm) refers to resistivity, d_k (cm) the thickness, L (cm) the length, and W_e (cm) the distance between the Ag-electrodes.

3. RESULTS AND DISCUSSION

3.1 Visual Examination

Figure 1a and b demonstrate the digital images of ZITO thin films in their as-deposited state and after annealing at 400 °C under forming gas atmosphere, respectively. The values given as inset on the upper left corners in Fig 1a indicate the employed substrate temperatures during depositions. It is obvious that the films exhibit visual transparency across all substrate temperatures suggesting that the influence of substrate temperature on visible transmittance is negligible. However, the film deposited at 150 °C (the one in the middle) appears slightly different than others, i.e., being particularly transparent, and colorless. It is apparent from Fig. 1b that the postgrowth annealing process can eliminate the partial coloration observed in the as-deposited samples. Further, the sample produced at 150 °C still looks the most transparent among others by visual inspection.

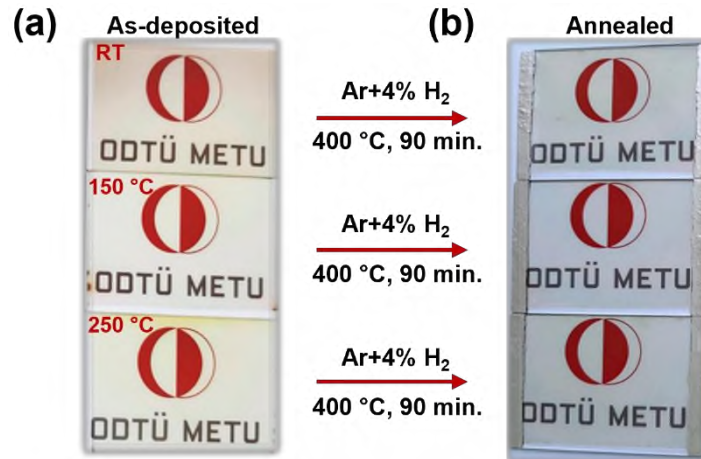


Figure 1. Digital images of ZITO thin films deposited at various substrate temperatures on 5 cm x 7.5 cm glass substrates, a) as-deposited, b) after annealing at 400 °C under Ar+4% H₂ atmosphere for 1.5 h

3.2 Structural Examination

Figure 2 (a) shows the XRD patterns of ZITO thin films deposited at various substrate temperatures. The broad and low intensity humps observed around $2\theta = 25^\circ - 35^\circ$, without any detectable peaks, indicate the amorphous nature of the ZITO samples, regardless of the deposition temperature. The existing literature on ZITO reveals inconsistent results about the onset temperature of crystallization [21, 31, 48, 52]. The formation of crystalline state is directly related to the substrate temperature, but it is also influenced by other parameters, such as film composition, sputtering power, and the use of either single alloyed target or co-sputtering for deposition. Numerous studies state that high Zn content in the composition induces amorphization in films [46, 52, 53]. This might be also valid for the current study due to the concentration of Zn-cation in the manufactured thin films, (See Table 1). However, our recent study on the combinatorial production of ZITO thin films revealed that this condition is not always true. In contrast, ZITO films with very high Zn component can display crystallization, whereas those with a lower zinc content may remain amorphous. [49]. Furthermore, the diffraction data of the annealed samples (Fig. 2b) indicates that the amorphous nature of the films can be maintained even after subjecting the samples to moderately high temperatures. These findings suggest that the film composition under consideration is highly resistant to crystallization and may be suitable for flexible or bendable applications [39]. Besides, the absence of grain boundaries can be advantageous for low sheet resistance transparent heaters due to high mobility of charge carriers without interruption of grain boundary barriers.

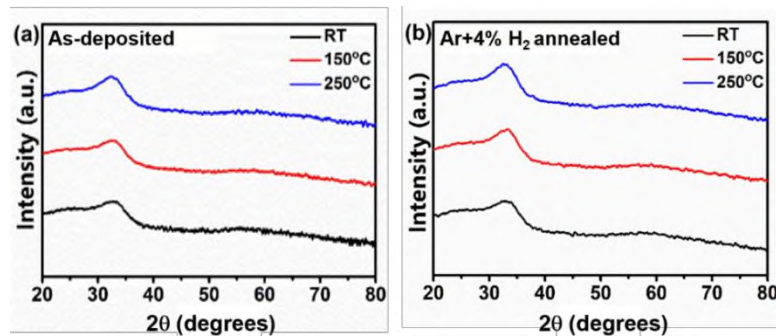


Figure 2. XRD patterns of a-ZITO thin films deposited at various substrate temperatures on 5 cm x 7.5 cm glass substrates, (a) as-deposited, (b) after annealing under Ar+4% H₂ atmosphere for 1.5 h at 400 °C

3.2 Morphological and Compositional Examination

Figures 3a1, b1, and c1 illustrate the high-magnification surface FE-SEM micrographs of a-ZITO thin films that were produced on substrates maintained at RT, 150 °C, and 250 °C, respectively. The inset images correspond to the low magnification, larger area observations of the same samples. Although the images of RT and 150 °C deposited thin films demonstrate some hill-like protrusions, the film surfaces can be acceptable as featureless in general. These formations are also visible from the 3D AFM surface topography images demonstrated in Figs. 3a5 and b5. It is apparent that the protrusions are much smaller in diameter (≤ 80 nm) in the RT deposited sample, but their areal density is high. On the contrary the diameters can approach 300 nm for 150 °C deposited sample, but they are highly dispersed. Moreover, the height of the hills on the surface of both samples are not greater than 25-30 nm. On the other hand, the surface of the sample deposited at 250 °C is free from these protrusions (see Figs. 3c1 and c5). Therefore, these formations may be attributed to low adatom mobility at lower substrate temperatures, lack of crystallinity and shadowing effects. According to the inset images given in Figs. 3a1, b1, and c1, it can be stated that the as-deposited a-ZITO samples are homogenous with no evidence of cracks, voids and peeling.

The root mean square (RMS) values of the as-deposited samples were calculated as 1.83, 3.12, and 0.453 nm over a $2 \mu\text{m} \times 2 \mu\text{m}$ surface area via AFM measurements, indicating the film's surfaces are practically smooth despite the presence of local hill-like feature formations. Figs. 3a2, b2, and c2 illustrate the surface FE-SEM images of samples after post-growth annealing. The high magnification SEM observation of the annealed samples did not provide significant detail about the effect of the heat treatments on surface morphology due to the featureless nature of the films. On the other hand, inset images revealed that the surface homogeneities were preserved after annealing. Additionally, 3D AFM surface images (Figs. 3a6 and 3b6) revealed that annealing had a noticeable effect on the protrusions present on the surface of as-deposited samples, leading to reduction in their number (for RT deposited sample) and decrease in sizes (for 150 °C deposited sample). Furthermore, the surface roughness decreased almost 50% for all samples with annealing. RMS values were identified as 0.808, 1.98, and 0.294 nm for RT, 150 °C, and 250 °C deposited thin films, respectively. These surface modifications probably stem from the surface reactions occurred at 400 °C annealing temperature. Obviously, increased smoothness is advantageous for mechanical and chemical inertness of a heater designed for use in ambient environments.

Figs. 3a3-4, b3-4, and c3-4 show the cross-sectional FE-SEM images of as-deposited and annealed samples. The thickness of the as deposited samples appears to be identical. This was achieved by tuning the deposition rates for all deposition temperatures. In addition, no alteration in the thickness was detected after annealing. Therefore, the electrothermal characteristics of the samples produced at various temperatures can be comparable. The cross-sections of both as-deposited and annealed thin films present no recognizable features, probably due to amorphous nature. Moreover, the inset images given in each figure imply that the films were obtained with uniform thickness and absence of any peeling from the substrate even after moderately high temperature annealing.

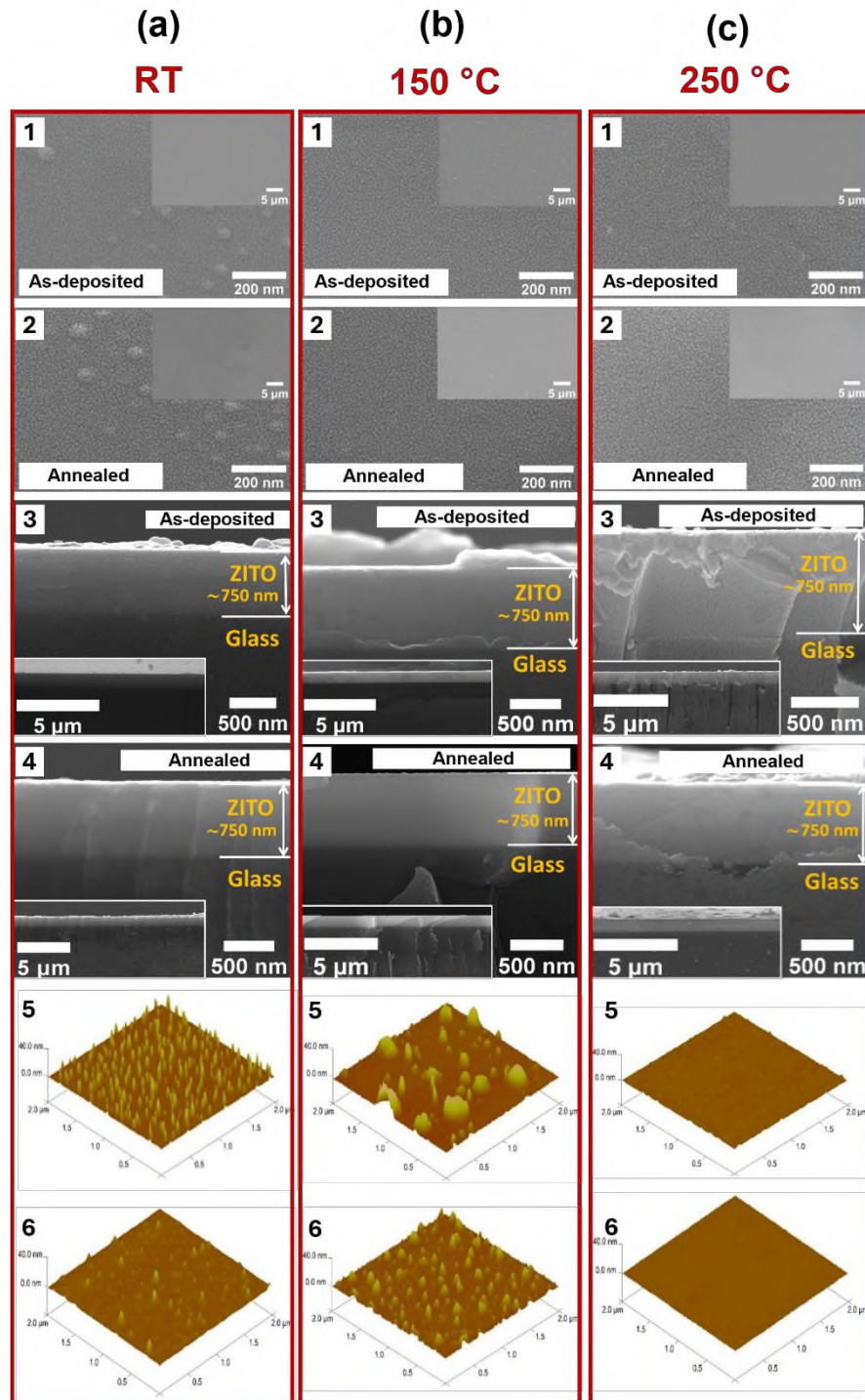


Figure 3. FE-SEM surface, through thickness and 3D AFM surface images of a) RT deposited, b) 150 °C deposited, c) 250 °C deposited a-ZITO thin films in as-deposited and annealed states (The surface SEM images and the insets were recorded at $\times 400000$ and $\times 10000$ magnifications, respectively. The cross-sectional SEM images and the insets were recorded at $\times 100000$ and $\times 10000$ magnifications, respectively)

Table 1. EDX analyses of a-ZITO thin films produced at various substrate temperatures and annealed under Ar+4% H₂ atmosphere for 1.5 h at 400 °C

Deposition temperature	As-deposited samples (at.%)			Postgrowth annealed samples (at.%)		
	Indium	Zinc	Tin	Indium	Zinc	Tin
RT	47.18	48.13	4.69	44.22	50.51	5.26
150 °C	46.76	45.84	7.39	41.73	51.93	6.34
250 °C	47.01	46.04	6.95	46.43	47.87	5.7

As discussed in Section 2.1, a-ZITO thin films were deposited on substrates held at RT, 150 °C, and 250 °C by sputtering of a 3'' target consists of In:Zn:Sn cation at.% of 44.5:49.6:5.9. Table 1 shows the atomic ratios of these cations measured in the as-deposited and annealed samples via EDX. The result shows that the as-deposited thin films are slightly enriched by In-cations (~47 at.%) compared to In-content (44.5 at.%) of the target composition. This enrichment was compensated by 1-2 at. % variations between the amount of Zn and Sn cations in the films as a function of used substrate temperatures. Considering the accuracy range of EDX method, it can be stated that the films obtained at various substrate temperatures displayed practically the same composition as the target. After annealing, the distribution of the constituent cations slightly modified and approximated to the desired chemical make-up. When compared to their as-deposited compositions, annealed thin films were slightly enriched by Zn and depleted by In. This suggests that the annealing temperature was high enough for diffusion and rearrangement of the elements in the films, however remains below threshold for crystallization.

3.3 Optical Examination

Fig. 4a demonstrates the transmittance spectra of as-deposited a-ZITO thin films as a function of substrate temperature. For visual aid, the threshold for 75% transmittance is indicated with a dashed red line and the visible range is marked with a shaded area. It can be inferred from the images that all films exhibited high transmittance (e.g. > 80%) in the visible range regardless of the deposition temperature. Furthermore, T_{vis} values of the samples deposited at RT, 150 °C, and 250 °C were calculated as 82.5 %, 85.9 %, and 84.0 %, respectively, as presented in Table 2.

Fig. 4b reveals that the postgrowth annealing has no significant impact on average visible transmittances of the films which were determined as 85.6%, 85.6%, and 85.5% (see Table 2). Similar observations, or even reductions in the optical transmittance of ZITO thin films annealed in a forming gas atmosphere have been reported by others [20, 21]. On the contrary, significant improvement in the visible region transmittance after Ar+H₂ atmosphere annealing have been observed for RT deposited ZITO thin films with various compositions [48]. Furthermore, the absorption edges of the films displayed changes depending on the substrate temperature employed during the deposition. In the as-deposited state, the absorption edges were found to be 377, 372, and 379 nm for RT, 150 °C, and 250 °C, respectively. Upon annealing under forming gas, a blue shift occurred, and the absorption edges of the annealed films were measured as 365, 364, and 371 nm. The shift towards near UV was attributed to an increase in carrier concentration [21]. As listed in Table 2, the sample deposited at 150 °C exhibited the highest band gap values of 3.17 eV in the as-deposited state and 3.26 eV after annealing. The broadening of the band gap after annealing was ascribed to increase in carrier concentration and generally defined by the Burstein–Moss effect [20, 54]. These results confirm that the manufactured a-ZITO thin films exhibit sufficient transparency and appropriate band gap for the targeted transparent heater applications.

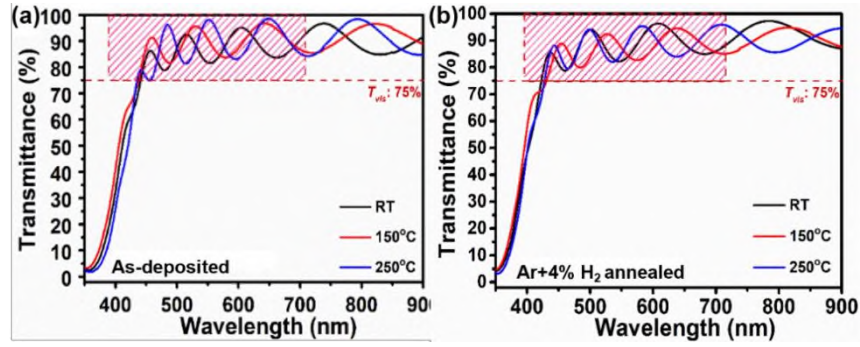


Figure 4. Transmittance spectra of a-ZITO thin films deposited at various substrate temperatures on 5 cm x 7.5 cm glass substrates: a) as-deposited and b) after annealing under Ar+4% H₂ atmosphere for 1.5 h at 400 °C (the shaded region in the figures denote the transmittance above 75% in the visible range and given for visual aid)

Table 2. Optical properties of a-ZITO thin films produced at various substrate temperatures and annealed under Ar+4% H₂ atmosphere for 1.5 h at 400 °C

Deposition temperature	As-deposited samples			Postgrowth annealed samples		
	T _{vis} (%)	Absorption edge (nm)	E _g (eV)	T _{vis} (%)	Absorption edge (nm)	E _g (eV)
RT	82.5	377	3.13	85.6	365	3.23
150 °C	85.9	372	3.17	85.6	364	3.26
250 °C	84.0	379	3.09	85.5	371	3.19

3.4 Electrical Examination

The thin films were subjected to Hall Effect measurements in the as-deposited and annealed states in order to determine the type of conductivity, sheet resistance (R_s , Ω/\square), carrier concentration (η , cm^{-3}), Hall mobility (μ , cm^2/Vs), and electrical resistivity (ρ , $\Omega\cdot\text{cm}$) of the produced samples. All samples showed n-type conductivity allowing the discussion of their electrical conductivity in terms of electron charge, carrier concentration, and mobility. Figures 5a-c presents the R_s , η , μ , and ρ as a function of substrate temperature for both as-deposited and annealed samples. In addition, Table 3 provides numerical values for these properties. The dependency of the electrical properties to deposition temperature is obvious from Figs. 5a and b and the results are consistent with the optical properties. The carrier concentration of the as-deposited samples first showed a slight increase (~8%) when the deposition temperature is raised from RT to 150 °C, but then substantially decreased (~55%) followed by the increase in substrate temperature. On the other hand, the mobility exhibited proportional dependence on temperature and raised from 36.77 cm^2/Vs to 42.01 cm^2/Vs for RT and 150 °C deposited samples and eventually reached 44.56 cm^2/Vs for the sample deposited at 250 °C. The high mobility of the films further indicates the absence of long-range order and grain boundaries in the as-deposited samples, both of these are known to adversely affect the mobility of charge carriers [55]. This direct correlation between the mobility and temperature may seem contradictory, as one would expect the lowest deposition temperature is usually associated with the more disordered structure, which should enhance the mobility. However, it is known that the mobility of the charge carriers in amorphous transparent conducting oxides not only affected by this factor but also affected from the ratio of cations, the corresponding local bonding and the presence of oxygen deficiencies in the structure [56, 57]. Further, 250 °C deposited sample exhibited the lowest carrier density among others, which might contribute to its high mobility value. Additionally, the sample deposited at 150 °C displayed the lowest R_s among the as-deposited samples (24.2 Ω/\square), compared to the values of 30 Ω/\square and 41.4 Ω/\square for the RT and 250 °C samples, respectively.

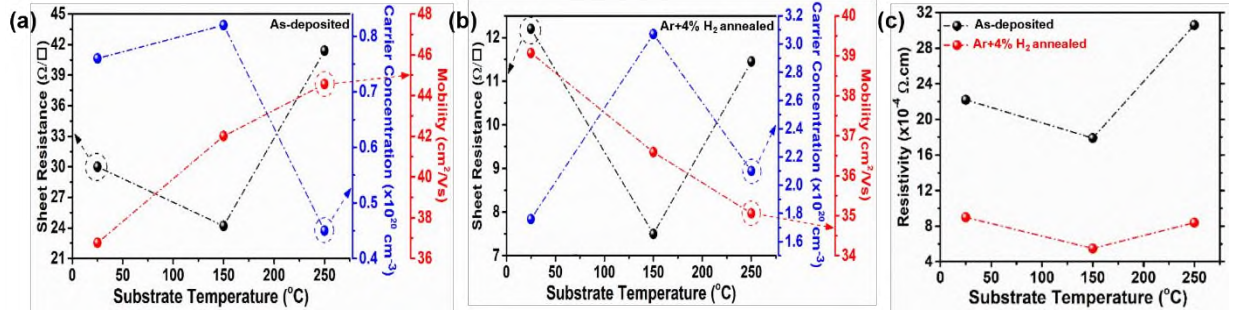


Figure 5. Electrical properties of a-ZITO thin films as a function of substrate temperature in as-deposited and post-growth annealed states: a) as-deposited sheet resistance, carrier concentration and mobility, b) annealed sheet resistance, carrier concentration and mobility, c) electrical resistivity in as-deposited and annealed states.

Table 3. Electrical properties of a-ZITO thin films produced at various substrate temperatures and annealed under Ar+4% H₂ atmosphere for 1.5 h at 400 °C

Sample		ρ^*10^{-4} (Ωcm)	R_s (Ω/\square)	η^*10^{20} (cm^{-3})	μ (cm^2/Vs)
As-deposited Samples	RT	22.2 ($\pm 1.5 \times 10^{-4}$)	30	0.76 ($\pm 2.5 \times 10^{-4}$)	36.77 ($\pm 1.1 \times 10^{-2}$)
	150 °C	17.9 ($\pm 2.5 \times 10^{-4}$)	24.2 ($\pm 5.7 \times 10^{-4}$)	0.82 ($\pm 5.7 \times 10^{-5}$)	42.01 ($\pm 2.0 \times 10^{-3}$)
	250 °C	30.6 ($\pm 8.6 \times 10^{-3}$)	41.4 ($\pm 1.1 \times 10^{-2}$)	0.45 ($\pm 4.9 \times 10^{-4}$)	44.56 ($\pm 3.8 \times 10^{-2}$)
Postgrowth Annealed Samples	RT	9.0 ($\pm 7.2 \times 10^{-4}$)	12.2 ($\pm 1.1 \times 10^{-3}$)	1.76 ($\pm 5.7 \times 10^{-4}$)	39.07 ($\pm 2.0 \times 10^{-2}$)
	150 °C	5.5 ($\pm 5.7 \times 10^{-5}$)	7.5	3.07 ($\pm 1.0 \times 10^{-3}$)	36.59 ($\pm 1.4 \times 10^{-2}$)
	250 °C	8.4 ($\pm 1.1 \times 10^{-4}$)	11.45	2.10 ($\pm 5.7 \times 10^{-4}$)	35.06 ($\pm 7.5 \times 10^{-3}$)

Fig. 5b and Table 3 illustrates the electrical properties of the samples, which underwent considerable modification after annealing in contrast to negligible change in the optical transmittance. In comparison to the as-deposited states, forming gas annealing enhanced the sheet resistance of all samples. Although the lowest R_s was achieved with the annealing of 150 °C deposited thin film (7.5 Ω/\square), the highest improvement as compared to as-deposited state was observed for 250 °C deposited sample with a reduction of 3.6-fold in its sheet resistance value (11.45 Ω/\square). In addition, RT deposited sample also showed a very low sheet resistance (12.21 Ω/\square) after thermal treatment. The enhancement in the R_s of thin films after post-growth annealing can primarily be attributed to a noticeable increase in their carrier concentrations. After annealing, the carrier concentrations of the samples deposited at RT, 150 °C, and 250 °C increased around 131%, 274%, and 366%, respectively. Ndione et al., stated that the conductivity of a-ZITO depend on the cation composition and partial pressure of oxygen during deposition [47]. Others emphasized the effect of electron, hole or oxygen vacancy formation as a result of the substitution of Zn²⁺ and Sn⁴⁺ into In³⁺ sites [58, 59]. Although the films in this study were produced under near-zero oxygen partial pressure and displayed similar cation compositions, the extend of atomic substitutions and the number of oxygen vacancies likely vary with the substrate temperature. Thus, the conductivity of as-deposited samples differs from each other. Further, the significant increase in the carrier concentrations with annealing can be attributed to the incorporation of hydrogen into the structure [60] as well as to the

suppression of localized defects and rearrangement of disordered charge distribution due to modification of amorphous network during annealing [61].

In contrast to the observations on the direct relationship between the mobility and substrate temperature for the as-deposited samples, the mobility of the films exhibited an inverse proportion with the employed deposition temperature for the films annealed at 400 °C. The highest mobility was achieved for the annealed state of the sample deposited at RT as 39.07 cm²/Vs. This value is higher than that of as-deposited counterpart. As the mobility of the films increased during film deposition under high purity Ar gas (practically $P_{O_2} \cong 0$) with an increasing deposition temperature, the enhancement of the mobility of the RT deposited thin film after Ar + H₂ (practically $P_{O_2} \cong 0$) annealing at 400 °C can be predicted. Interestingly, other samples exhibited decline in mobility after annealing. The annealed samples deposited at 150 °C and 250 °C exhibited mobility values of 36.59 cm²/Vs and 35.06 cm²/Vs, respectively. This decrease in the mobilities of 150 °C and 250 °C deposited samples after annealing can be ascribed to significant increase in their carrier concentration (274% and 366%, respectively) due to inverse relationship between these two properties. However, it is important to highlight that the mobility in amorphous oxide semiconductors depends on various parameters such as bonding energy difference of oxygen with the constituent cations, metal-oxygen local coordination's and the change of coordination states with annealing, modifications in the local distortions of metal-oxygen polyhedrons, formation of MO₆ chain structure and random distribution of MO₄ tetrahedrons, and structural differences at local or medium-range ordering [56]. Therefore, the aforementioned discussion on the mobility of annealed a-ZITO thin films just depends on the experimental observations and may require further investigation. In contrast, this research centers on the fabrication of TFTHs with a specific ZITO composition, highlighting that forming gas annealing serves as a beneficial technique for enhancing the electrical properties of the samples.

Figure 5c demonstrates the electrical resistivity of the annealed samples compared to their as-deposited state. The specific values can be followed from Table 3. The lowest resistivity was achieved via the annealing of 150 °C deposited sample as $5.5 \times 10^{-4} \Omega \cdot \text{cm}$. The conductivity of the films was calculated using $\sigma = 1/\rho$ relation and determined as 1111 S/cm, 1818 S/cm, and 1190 S/cm, respectively for RT, 150 °C and 250 °C deposited samples. Accordingly, the FOM values were obtained as $11.79 \times 10^{-3} \Omega^{-1}$, $34.21 \times 10^{-3} \Omega^{-1}$, and $17.35 \times 10^{-3} \Omega^{-1}$ as in the same order.

3.5 Electrothermal Examination

Post-growth annealed a-ZITO TFTHs were subjected to 12 V to assess their heating response. The resulting data were plotted as a function of time and presented in Fig. 6a. As illustrated, all samples exhibited an increasing trend in terms of average surface temperature with the application of 12 V. Among these, the highest heating rate and maximum temperature was observed for the sample deposited at 150 °C. The response time i.e., the time that elapsed to attain 90% of the surface saturation temperature was measured as 102 s. Additionally, the heating response of 150 °C produced a-ZITO thin film to various applied voltage input was examined with the sample kept under ambient conditions. Fig. 6b shows the response of as-deposited thin film to 3, 6, 9, and 12 V inputs. The insets display the maximum average surface temperature of the sample after 500 seconds, along with the corresponding infrared camera image of the surface. As is obvious from the shape of the curves that the surface temperature of the TFTH initially increases and then saturates at a higher temperature. Further, the saturation temperature was found to increase proportional to the increasing input voltage. For the measurements conducted at applying 3, 6, 9, and 12 V, the mean saturation temperatures were recorded as 30, 47, 69, and 89 °C, respectively. This almost corresponds to 20 °C increase in the maximum achievable temperature for each 3V increments, suggesting that the saturation temperature depends on the power supplied to the heater [54].

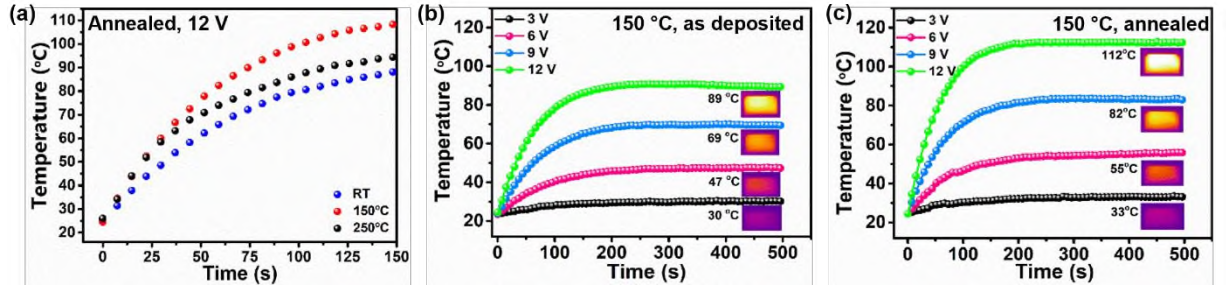


Figure 6. Electrothermal responses of a) post-growth annealed a-ZITO thin films to 12 V input, 150 °C deposited a-ZITO thin film to various applied voltages b) as-deposited, c) annealed (the inset images given in each figure refers to the thermal camera image of the sample at the corresponding saturation temperature)

Figure 6c displays the results of the same tests conducted using the annealed sample. In this case, the saturation temperatures were measured as 33, 55, 82, and 112 °C for input voltages of 3, 6, 9, and 12 V, respectively. These improvements in the heating behavior are expected as the annealing process significantly reduced the sheet resistance of the samples. In addition, the response time of the samples in the case of 6, 9, and 12 V inputs were calculated as 124, 114, and 102 s. These can be considered as moderate values for transparent heaters and might be attributed to sluggish heat conduction in the case of amorphous thin films [62]. On the other hand, the decreasing trend in the response time of the sample with the increasing input voltage can be defined by the increase in the specific heat of the film with increasing input power [63].

Electrothermal response of 150 °C deposited and annealed a-ZITO TFTH with respect to various electrical input conditions are illustrated in Fig. 7a, b and c. The behavior of the sample against voltage increase (+2V in every 60 s) up to 12 V is displayed in Fig. 7a. It is obvious that the sample exhibited linear response to voltage increases beyond 4 V. Further, the surface temperature enhanced after each increment as can be followed from the inset images. At an input of 12 V, the temperature reached approximately 96 °C after 60 s, and the sample demonstrated rapid cooling when the power supply was turned off.

The stability test was conducted by observing the change in the surface temperature for an extended period of time (e.g., 3600 s) under a specified voltage input. The test was performed at 60 °C surface temperature, achieved by applying 7 V, as shown in Fig. 7b. Under ambient atmospheric conditions, the deviation in temperature was negligible (± 0.4 °C) indicating stable performance of the a-ZITO TFTH. The spatial distribution or the homogeneity of the surface temperature was calculated to be 19.66%. The uniformity value of the current TFTH is superior compared to that of wire-patterned deicing system suggested for car windshields and metallic quantum nanoparticle layered Ni/FTO transparent heaters [64, 65]. Moreover, the sample provided almost equivalent uniformity to that of NiCr/FTO (19.2 %) and bare FTO (19.7 %), but poorer homogeneity than Cr/FTO (14.65 %), AZO/SiO₂ (13.66 %), FTO/AZO (11.42 %), and AZO (17.70 %) TFTHs reported in literature [51, 54, 65, 66].

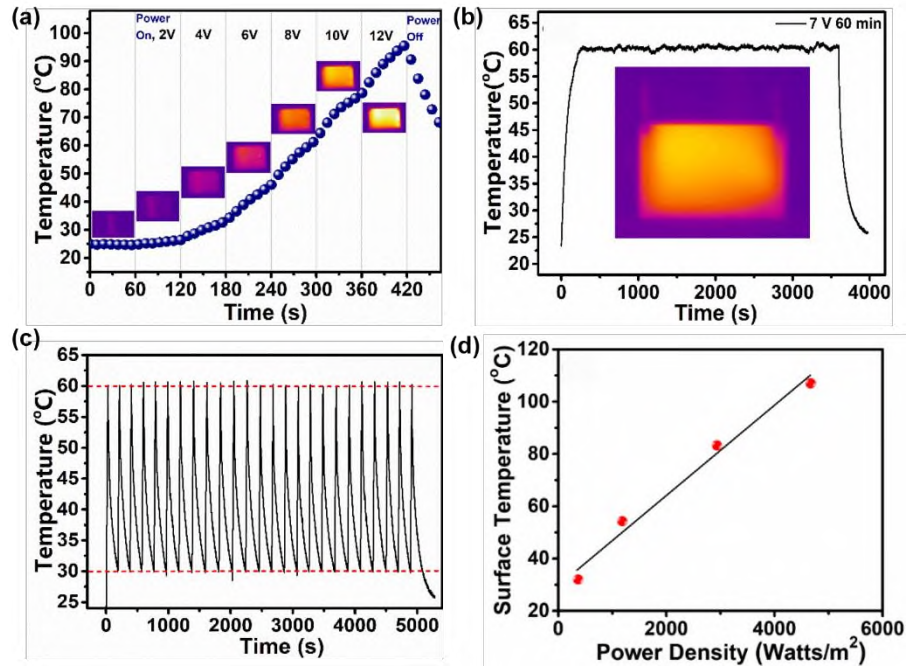


Figure 7. Electrothermal response of 150 °C deposited and forming gas annealed a-ZITO thin film to a) accumulative input voltage, b) constant input voltage stability, c) cyclic input voltage response, d) power density vs. surface saturation temperature relation (the inset images given in (a) and (b) refers to the thermal camera image of the sample at the corresponding temperature)

The cyclic voltage response of the sample was tested using 0-12 V on/off condition and illustrated in Fig. 7c. The surface temperature of the TFTH was first allowed to reach 60 °C by implementing 12 V, then the power supply was turned off to allow the heater to cool to 30 °C. This heating/cooling cycle was repeated 25 times. The horizontal red dashed lines in the figure show the upper and lower limits of the test. The peak temperature consistently attained around 25 s, indicating a heating rate of 1.2 °C/s.

The surface saturation temperature of the heater was recorded as a function of power density (electrical power/total active area) for 3, 6, 9, and 12 V inputs. The corresponding data points along with the fitted line plot is presented in Fig. 7d. Using the linear relationship between the power density and achieved saturation temperatures, the thermal resistance of the sample was calculated as 181.7 °C.cm²/Watt from dT/dP . In addition, the power consumption and power density of the sample (with an active area of 32.2 cm²) was calculated to be 3.95 W and 0.4635 Watt/cm², respectively in case of 12 V input. A transparent heater is expected to provide heating power density values around 0.4 Watt/cm² to meet specifications for deicing applications in sea or air vehicles [67]. This implies that the a-ZITO heater prepared in this study has the potential to be used as an effective TFTHs device.

Deicing efficiency of 150 °C deposited and annealed a-ZITO TFTH was examined under different voltage input conditions and data are displayed in Fig. 8a. The maximum achieved temperature and the corresponding time for complete evaporation of water from the surface are presented as inset next to each curve. The overall deicing and complete evaporation time decreased with the increasing voltage input, as expected. Water droplets disappeared from the heater surface in 299, 195, and 173 s for 6, 9, and 12 V input. On the contrary, the maximum average surface temperature increased with the applied voltage reaching 50, 57, and 92 °C. For 12 V input, the camera recorded a surface temperature of 0 °C after ~23 s, and 30 °C in 50 s. Beyond this point, the temperature increased almost linearly with a heating rate of 0.68 °C/s. The inset images refer to the captures of the heater's surface by the camera during deicing at 0, 80, and 173 s under 12 V. The first image reveals a homogenous color resembling the initial condition of -40 °C. After 80 s, the temperature reached 50 °C. The dark spots highlight the remaining water droplets. After a while,

all the droplets evaporated, and the surface displayed a more homogenous temperature distribution as can be seen in the final inset image.

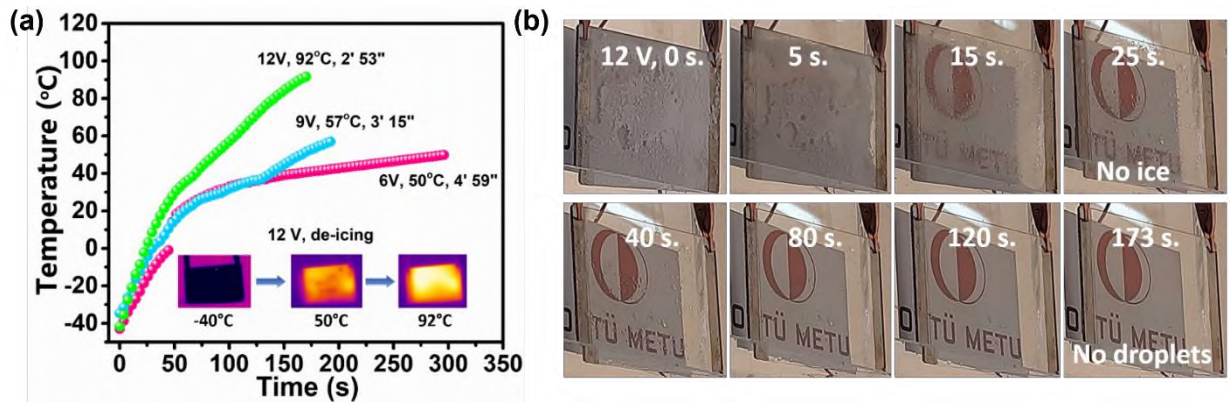


Figure 8. Deicing efficiency of 150 °C deposited 50 x 75 mm² a-ZITO thin film a) heating curves for 6, 9, and 12 V input starting from -40 °C, b) real-time digital deicing images of the heater as a function of time (inset images in (a) refer to the thermal camera captures of the sample during deicing at time 0, 80, and 173 s for 12 V input)

The digital images of the a-ZITO TFTH were collected at some points during the deicing process and presented in Fig. 8b in case of 12 V input. As can be seen from images, there is no clear visibility at the beginning due to condensed ice on the surface. However, a rapid melting occurred within 15 s improving the visibility as the ice layer melts. The translucent state turned to transparent almost within one minute. After this point the remaining droplets on the surface continued to evaporate and it took almost 3 min to remove all droplets from the surface via evaporation.

4. CONCLUSIONS

ZnO-In₂O₃-SnO₂ thin film transparent heaters were manufactured using a 3" sputtering target with a specific cation composition of 49.6 at.% Zn, 44.5 at.% In, and 5.9 at.% Sn. The effects of substrate temperature and post-growth annealing on structural, morphological, optical, and electrical properties were investigated. The structural examination showed that the films were amorphous regardless of the substrate temperature in as-deposited state and this structure was maintained after annealing. Annealing under forming gas slightly increased the visible transmittance ($T_{vis} \sim 85\%$) but substantially modified the electrical properties. The sample produced at a substrate temperature of 150 °C exhibited the lowest sheet resistance value (7.5 Ω/\square) among the others. Electrothermal characterization results demonstrated that a-ZITO TFTHs exhibit power input-dependent, reproducible heating behavior with excellent stability and temperature homogeneity. The thermal resistance, power consumption, and areal power density of 150 °C deposited TFTH with an active area of 32.2 cm² were determined as 181.7 °C.cm²/Watt, 3.95 W, and 0.4635 Watt/cm² in case of 12 V input, respectively. Furthermore, this heater presented an outstanding deicing ability where defrosting and liquid phase removal steps were completed below 3 minutes with a heating rate of 0.68 °C/s. These findings revealed that the a-ZITO TFTHs produced in this study are suitable for various commercial defogging/deicing applications and their electrothermal properties can be tuned easily via modification of the substrate temperature.

Declaration of Ethical Standards

The authors declare that they have carried out this completely original study by adhering to all ethical rules including authorship, citation and data reporting

Credit Authorship Contribution Statement

H.A: Funding acquisition, Project administration, Supervision, Investigation, Methodology, Writing-review & editing, **H.A.C:** Investigation, Data Curation, **B.K:** Data Curation, Writing-review & editing, **T.Ö:** Funding acquisition, Conceptualization, Supervision

Declaration of Competing Interest

The authors declare that they have no conflict of interest.

Data Availability

Data available on request from the author.

Acknowledgements

This study was produced from the MSc thesis of Hilal Aybike CAN and supported financially by the Scientific and Technological Research Council of Turkey (TÜBİTAK; Project Number: 118M013), for which the authors are thankful.

REFERENCES

- [1] S.P. Harvey, K.R. Poeppelmeier, and T.O. Mason, "Subsolidus Phase Relationships in the ZnO–In₂O₃–SnO₂ System," *Journal of the American Ceramic Society*, vol. 91, no. 11, pp. 3683-3689, 2008.
- [2] C.A. Hoel, T.O. Mason, J.-F. Gaillard, and K.R. Poeppelmeier, "Transparent Conducting Oxides in the ZnO-In₂O₃-SnO₂ System," *Chemistry of Materials*, vol. 22, no. 12, pp. 3569-3579, 2010.
- [3] T. Jantzen, K. Hack, E. Yazhenskikh, and M. Müller, "Thermodynamic assessment of oxide system In₂O₃-SnO₂-ZnO," *Chimica Techno Acta*, vol. 5, no. 4, pp. 166-188, 2018.
- [4] M.H. Cho, C.H. Choi, and J.K. Jeong, "Recent progress and perspectives on atomic-layer-deposited semiconducting oxides for transistor applications," *Journal of the Society for Information Display*, vol. 30, no. 3, pp. 175-197, 2022.
- [5] I. Noviyana, A.D. Lestari, M. Putri, M.-S. Won, J.-S. Bae, Y.-W. Heo, and H.Y. Lee, "High mobility thin film transistors based on amorphous indium zinc tin oxide," *Materials*, vol. 10, no. 7, pp. 702, 2017.
- [6] J. Sheng, T. Hong, D. Kang, Y. Yi, J.H. Lim, and J.-S. Park, "Design of InZnSnO semiconductor alloys synthesized by supercycle atomic layer deposition and their rollable applications," *ACS applied materials & interfaces*, vol. 11, no. 13, pp. 12683-12692, 2019.
- [7] T. Kim, C.H. Choi, J.S. Hur, D. Ha, B.J. Kuh, Y. Kim, M.H. Cho, S. Kim, and J.K. Jeong, "Progress, challenges, and opportunities in oxide semiconductor devices: a key building block for applications ranging from display backplanes to 3D integrated semiconductor chips," *Advanced Materials*, vol. 35, no. 43, pp. 2204663, 2023.
- [8] T.E. Taouririt, A. Meftah, N. Sengouga, M. Adaika, S. Chala, and A. Meftah, "Effects of high-k gate dielectrics on the electrical performance and reliability of an amorphous indium–tin–zinc–oxide thin film transistor (a-ITZO TFT): an analytical survey," *Nanoscale*, vol. 11, no. 48, pp. 23459-23474, 2019.
- [9] H. Yang, W. Yang, J. Su, and X. Zhang, "Enhancement-mode thin film transistor using amorphous phosphorus-doped Indium–Zinc–Tin-Oxide channel layer," *Materials Science in Semiconductor Processing*, vol. 137, no. pp. 106228, 2022.
- [10] Y.G. Bak, J.W. Park, Y.J. Park, M.Z. Ansari, S. NamGung, B.Y. Cho, S.-H. Kim, and H.Y. Lee, "In-Zn-Sn-O thin film based transistor with high-k HfO₂ dielectric," *Thin Solid Films*, vol. 753, no. pp. 139290, 2022.

- [11] Y. Li, S. Yin, Y. Du, H. Zhang, J. Chen, Z. Wang, S. Wang, Q. Qin, M. Zhou, and L. Li, "Liquid-metal based flexible a-IZTO ultrathin films for electrical and optical applications," *Nanoscale*, vol. 14, no. 45, pp. 16797-16805, 2022.
- [12] C.P.T. Nguyen, T.T. Trinh, J. Raja, A.H.T. Le, K. Jang, Y.-J. Lee, and J. Yi, "High performance non-volatile memory with the control of charge trapping states in an amorphous InSnZnO active channel," *Semiconductor Science and Technology*, vol. 30, no. 7, pp. 075009, 2015.
- [13] J.-H. Bae, J.-M. Moon, S.W. Jeong, J.-J. Kim, J.-W. Kang, D.-G. Kim, J.-K. Kim, J.-W. Park, and H.-K. Kim, "Transparent conducting indium zinc tin oxide anode for highly efficient phosphorescent organic light emitting diodes," *Journal of The Electrochemical Society*, vol. 155, no. 1, pp. J1, 2007.
- [14] G.-S. Heo, Y. Matsumoto, I.-G. Gim, J.-W. Park, K.-Y. Kim, and T.-W. Kim, "Fabrication of cosputtered Zn-In-Sn-O films and their applications to organic light-emitting diodes," *Solid state communications*, vol. 149, no. 41-42, pp. 1731-1734, 2009.
- [15] T.-W. Kim, G.-S. Heo, H.-S. Kim, and J.-H. Lee, "Combinatorial exploration of new transparent conducting oxide films by using radio frequency sputtering and their application in optoelectronic devices," *MRS Online Proceedings Library (OPL)*, vol. 1425, no. pp. mrsf11-1425-uu01-04, 2012.
- [16] S.W. Heo, E.J. Lee, Y.W. Han, Y.S. Lee, W.J. Lee, S.-H. Choa, Y.S. Kim, and D.K. Moon, "Improved performance of flexible polymer light emitting diodes with an indium-zinc-tin-oxide transparent anode by controlling the thermal treatment temperature," *Journal of industrial and engineering chemistry*, vol. 53, no. pp. 68-76, 2017.
- [17] H.-K. Jeong and K.-M. Lee, "Effects of flow rate of atmosphere gases on the characteristics of Zn-doped ITO (ZITO) thin films for organic light emitting diodes," *Functional Materials Letters*, vol. 8, no. 03, pp. 1540007, 2015.
- [18] H.J. Lee, I. Noviyana, C.Y. Koo, J.-A. Lee, J.-J. Kim, A.D. Lestari, Y. Jeong, Y. Lee, and H.Y. Lee, "Organic Photovoltaics with Non-Stoichiometric InZnSnO Thin Film Cathodes," *Journal of Nanoscience and Nanotechnology*, vol. 17, no. 7, pp. 4822-4826, 2017.
- [19] H.J. Lee, I. Noviyana, M. Putri, C.Y. Koo, J.-A. Lee, J.-J. Kim, Y. Jeong, Y. Lee, and H.Y. Lee, "DC Magnetron Sputtered IZTO Thin Films for Organic Photovoltaic Application," *Journal of Nanoscience and Nanotechnology*, vol. 18, no. 2, pp. 1270-1273, 2018.
- [20] M. Putri, K.H. Kim, C.Y. Koo, J.-A. Lee, J.-J. Kim, I.D. Baikie, A.C. Grain, and H.Y. Lee, "Effect of annealing treatment on the properties of stoichiometric indium zinc tin oxide (IZTO) thin films," *Journal of Nanoelectronics and Optoelectronics*, vol. 12, no. 6, pp. 611-616, 2017.
- [21] H.C. Ma, Damisih, M. Putri, J.H. Cheon, J.H. Kim, and H.Y. Lee, "The effect of post-annealing treatment on the characteristics of a dye-sensitized solar cell with an indium zinc tin oxide electrode," *Journal of the Korean Physical Society*, vol. 61, no. pp. 1994-1999, 2012.
- [22] J.-D. Cho, Y.-B. Kim, G.-S. Heo, E.-M. Kim, and J.-W. Hong, "Optimization of Electro-Optical Properties of Acrylate-based Polymer-Dispersed Liquid Crystals for use in Transparent Conductive ZITO/Ag/ZITO Multilayer Films," *Applied Chemistry for Engineering*, vol. 31, no. 3, pp. 291-298, 2020.
- [23] E.M. Kim, I.-S. Choi, J.-P. Oh, Y.-B. Kim, J.-H. Lee, Y.-S. Choi, J.-D. Cho, Y.-B. Kim, and G.-S. Heo, "Transparent conductive ZnInSnO-Ag-ZnInSnO multilayer films for polymer dispersed liquid-crystal based smart windows," *Japanese Journal of Applied Physics*, vol. 53, no. 9, pp. 095505, 2014.
- [24] S. Syed Feroze Hussain and D. Thiripurasundari, "A review on optically transparent antenna fabricated with conductive nano-material oxides," *Journal of Electronic Materials*, vol. 51, no. 12, pp. 6707-6734, 2022.
- [25] H.Y. Lee, I.J. Yang, J.-H. Yoon, S.-H. Jin, S. Kim, and P.K. Song, "Thermoelectric properties of zinc-doped indium tin oxide thin films prepared using the magnetron co-sputtering method," *Coatings*, vol. 9, no. 12, pp. 788, 2019.
- [26] J.-A. Lee, Y.-W. Heo, J.-H. Lee, H.Y. Lee, and J.-J. Kim, "Structural and optical characteristics of Zn-rich In₂O₃-SnO₂-ZnO (ITZO) thin films prepared by radio frequency magnetron sputtering," *Journal of Nanoelectronics and Optoelectronics*, vol. 12, no. 6, pp. 598-601, 2017.

- [27] C.W. Ow-Yang, H.-y. Yeom, and D.C. Paine, "Fabrication of transparent conducting amorphous Zn-Sn-In-O thin films by direct current magnetron sputtering," *Thin Solid Films*, vol. 516, no. 10, pp. 3105-3111, 2008.
- [28] D.E. Proffit, S.P. Harvey, A. Klein, R. Schafrank, J.D. Emery, D.B. Buchholz, R.P. Chang, M.J. Bedzyk, and T.O. Mason, "Surface studies of crystalline and amorphous Zn-In-Sn-O transparent conducting oxides," *Thin Solid Films*, vol. 520, no. 17, pp. 5633-5639, 2012.
- [29] Y.R. Denny, S. Seo, K. Lee, S.K. Oh, H.J. Kang, S. Heo, J.G. Chung, J.C. Lee, and S. Tougaard, "Effects of cation compositions on the electronic properties and optical dispersion of indium zinc tin oxide thin films by electron spectroscopy," *Materials Research Bulletin*, vol. 62, no. pp. 222-231, 2015.
- [30] H.C. Ma, F. Finanda, J.-J. Kim, and H.Y. Lee, "Effect of composition in transparent conducting indium Zinc Tin Oxide thin films deposited by RF magnetron sputtering," *Journal of nanoelectronics and optoelectronics*, vol. 7, no. 5, pp. 483-487, 2012.
- [31] M. Putri, C.Y. Koo, J.-A. Lee, J.-J. Kim, and H.Y. Lee, "Transparent conducting indium zinc tin oxide thin films with low indium content deposited by radio frequency magnetron sputtering," *Thin Solid Films*, vol. 559, no. pp. 44-48, 2014.
- [32] P. Janicek, M. Putri, K.H. Kim, H.J. Lee, M. Bouska, S. Šlang, and H.Y. Lee, "Spectroscopic Ellipsometry Characterization of As-Deposited and Annealed Non-Stoichiometric Indium Zinc Tin Oxide Thin Film," *Materials*, vol. 14, no. 3, pp. 578, 2021.
- [33] K.H. Kim, M. Putri, H.J. Lee, C.Y. Koo, J.-A. Lee, J.-J. Kim, and H.Y. Lee, "Non-Stoichiometric Indium Zinc Tin Oxide Thin Films Prepared by RF Magnetron Sputtering," *Journal of Nanoelectronics and Optoelectronics*, vol. 10, no. 4, pp. 541-545, 2015.
- [34] E.M. Kim, J.-P. Oh, T.-W. Ha, Y.-B. Kim, T.-W. Kim, and G.-S. Heo, "Physical stability against hydrogen plasma for ZnInSnO thin films deposited by combinatorial RF magnetron sputtering," *Japanese Journal of Applied Physics*, vol. 55, no. 12, pp. 125801, 2016.
- [35] D.E. Proffit, T. Philippe, J.D. Emery, Q. Ma, B.D. Buchholz, P.W. Voorhees, M.J. Bedzyk, R.P. Chang, and T.O. Mason, "Thermal stability of amorphous Zn-In-Sn-O films," *Journal of Electroceramics*, vol. 34, no. pp. 167-174, 2015.
- [36] G.-S. Heo, I.-G. Gim, H.-K. Lee, J.-H. Song, and T.-W. Kim, "Investigation of bending stability of amorphous Zn-In-Sn-O thin films on flexible poly (ether sulfone) substrates," *Japanese Journal of Applied Physics*, vol. 49, no. 3R, pp. 031104, 2010.
- [37] Y.S. Kim, W.J. Hwang, K.T. Eun, and S.-H. Choa, "Mechanical reliability of transparent conducting IZTO film electrodes for flexible panel displays," *Applied surface science*, vol. 257, no. 18, pp. 8134-8138, 2011.
- [38] Y.S. Kim, S.-I. Oh, and S.-H. Choa, "Mechanical integrity of flexible In-Zn-Sn-O film for flexible transparent electrode," *Japanese Journal of Applied Physics*, vol. 52, no. 5S1, pp. 05DA17, 2013.
- [39] J.Y. Choi, I.P. Park, and S.W. Heo, "Ultra-flexible organic solar cell based on indium-zinc-tin oxide transparent electrode for power source of wearable devices," *Nanomaterials*, vol. 11, no. 10, pp. 2633, 2021.
- [40] Y.S. Kim, E.K. Lee, K. Eun, and S.-H. Choa, "Electromechanical properties of amorphous In-Zn-Sn-O transparent conducting film deposited at various substrate temperatures on polyimide substrate," *Japanese Journal of Applied Physics*, vol. 54, no. 9, pp. 095501, 2015.
- [41] K.-D. Li, P.-W. Chen, and K.-S. Chang, "Low-temperature deposition of transparent conducting films applied to flexible electrochromic devices," *Materials*, vol. 14, no. 17, pp. 4959, 2021.
- [42] J.Y. Choi, I.P. Park, and S.W. Heo, "Ultra-flexible organic photovoltaics with low-temperature deposited IZTO on a cyclic polymer substrate having excellent mechanical properties," *ACS Applied Materials & Interfaces*, vol. 13, no. 43, pp. 51289-51296, 2021.
- [43] S. Biswas, Y. Lee, H. Jang, S. Han, and H. Kim, "Improved mechanical stability of indium zinc tin oxide based flexible transparent electrode through interlayer treatment," *Journal of Applied Polymer Science*, vol. 140, no. 1, pp. e53251, 2023.

- [44] X. Jiang, S. Long, G. Zhu, H. Xu, J. Song, X. Zhang, Y. Zhao, T. Wei, N. Guo, and Y. Gong, "Preparation and Properties of Izto Ceramic Target by Cold Sintering," *Available at SSRN 4255408*, vol., no.,
- [45] I. Saadeddin, H.S. Hilal, R. Decourt, G. Campet, and B. Pecquenard, "Indium oxide co-doped with tin and zinc: A simple route to highly conducting high density targets for TCO thin-film fabrication," *Solid state sciences*, vol. 14, no. 7, pp. 914-919, 2012.
- [46] G.-S. Heo, I.-G. Gim, J.-W. Park, K.-Y. Kim, and T.-W. Kim, "Effects of substrate temperature on properties of ITO–ZnO composition spread films fabricated by combinatorial RF magnetron sputtering," *Journal of Solid State Chemistry*, vol. 182, no. 10, pp. 2937-2940, 2009.
- [47] P.F. Ndione, A. Zakutayev, M. Kumar, C. Packard, J. Berry, J. Perkins, and D. Ginley, "Tuning the physical properties of amorphous In–Zn–Sn–O thin films using combinatorial sputtering," *MRS Communications*, vol. 6, no. 4, pp. 360-366, 2016.
- [48] H.A. Can, T. Öztürk, and H. Akyıldız, "A combinatorial study on ZnO–In₂O₃–SnO₂ system: The effects of different postgrowth annealing conditions on optical and electrical properties," *Journal of Alloys and Compounds*, vol. 924, no. pp. 166591, 2022.
- [49] H.A. Can, T. Öztürk, and H. Akyıldız, "Effect of deposition parameters on optical and electrical properties of ZnO–In₂O₃–SnO₂ thin films," *Materials Chemistry and Physics*, vol. 296, no. pp. 127256, 2023.
- [50] D. Sari, Z.C. Torunoglu, Y.E. Kalay, and T. Ozturk, "Preparation of La_{0.8}Sr_{0.2}CoO_{3-δ} sputtering targets using a deformable compaction die," *Ceramics International*, vol. 43, no. 17, pp. 15185-15188, 2017.
- [51] B. Tönbul, H.A. Can, T. Öztürk, and H. Akyıldız, "Solution processed glass/fluorine-doped tin oxide/aluminum-doped zinc oxide double layer thin films for transparent heater and near-infrared reflecting applications," *Journal of Sol-Gel Science and Technology*, vol. 99, no. 3, pp. 482-496, 2021.
- [52] H.C. Ma, J.-J. Kim, and H.Y. Lee, "The electrical and optical properties of indium zinc tin oxide thin films with different Sn/Zn ratio," *Thin Solid Films*, vol. 520, no. 10, pp. 3741-3745, 2012.
- [53] T. Minami, T. Yamamoto, Y. Toda, and T. Miyata, "Transparent conducting zinc-co-doped ITO films prepared by magnetron sputtering," *Thin Solid Films*, vol. 373, no. 1-2, pp. 189-194, 2000.
- [54] H.A. Can, B. Tönbul, F. Pişkin, T. Öztürk, and H. Akyıldız, "Processing optimization of SiO₂-capped aluminum-doped ZnO thin films for transparent heater and near-infrared reflecting applications," *Journal of Materials Science: Materials in Electronics*, vol. 32, no. pp. 5116-5137, 2021.
- [55] P. Pujar, S. Gandla, D. Gupta, S. Kim, and M.G. Kim, "Trends in low-temperature combustion derived thin films for solution-processed electronics," *Advanced Electronic Materials*, vol. 6, no. 10, pp. 2000464, 2020.
- [56] R. Khanal, D.B. Buchholz, R.P. Chang, and J.E. Medvedeva, "Composition-dependent structural and transport properties of amorphous transparent conducting oxides," *Physical Review B*, vol. 91, no. 20, pp. 205203, 2015.
- [57] A. Zhussupbekova, A. Kaisha, R.K. Vijayaraghavan, K. Fleischer, I.V. Shvets, and D. Caffrey, "Importance of Local Bond Order to Conduction in Amorphous, Transparent, Conducting Oxides: The Case of Amorphous ZnSnO_y," *ACS applied materials & interfaces*, vol. 11, no. 47, pp. 44399-44405, 2019.
- [58] K.-D. Li and K.-S. Chang, "Effects of Zn ratio tuning on the structural and transport properties of amorphous indium zinc tin oxide thin films," *Journal of Electronic Materials*, vol. 49, no. 12, pp. 7336-7342, 2020.
- [59] P.-Y. Liao, T.-C. Chang, W.-C. Su, Y.-J. Chen, B.-W. Chen, T.-Y. Hsieh, C.-Y. Yang, Y.-Y. Huang, H.-M. Chang, and S.-C. Chiang, "Effect of mechanical-strain-induced defect generation on the performance of flexible amorphous In–Ga–Zn–O thin-film transistors," *Applied Physics Express*, vol. 9, no. 12, pp. 124101, 2016.

- [60] T. Kamiya, K. Nomura, and H. Hosono, "Origins of high mobility and low operation voltage of amorphous oxide TFTs: Electronic structure, electron transport, defects and doping," *Journal of display Technology*, vol. 5, no. 7, pp. 273-288, 2009.
- [61] J.E. Medvedeva, D.B. Buchholz, and R.P. Chang, "Recent advances in understanding the structure and properties of amorphous oxide semiconductors," *Advanced Electronic Materials*, vol. 3, no. 9, pp. 1700082, 2017.
- [62] L. Chen, N. Kumari, and Y. Hou, "Thermal resistances of crystalline and amorphous few-layer oxide thin films," *AIP Advances*, vol. 7, no. 11, 2017.
- [63] P. Nath and K. Chopra, "Thermal conductivity of amorphous vs crystalline Ge and GeTe films," *Japanese Journal of Applied Physics*, vol. 13, no. S1, pp. 781, 1974.
- [64] C. Baldasseroni, D. Queen, D.W. Cooke, K. Maize, A. Shakouri, and F. Hellman, "Heat transfer simulation and thermal measurements of microfabricated x-ray transparent heater stages," *Review of Scientific Instruments*, vol. 82, no. 9, 2011.
- [65] C. Hudaya, B.J. Jeon, and J.K. Lee, "High thermal performance of SnO₂: F thin transparent heaters with scattered metal nanodots," *ACS Applied Materials & Interfaces*, vol. 7, no. 1, pp. 57-61, 2015.
- [66] B. Tönbul, H.A. Can, T. Öztürk, and H. Akyıldız, "Solution processed aluminum-doped ZnO thin films for transparent heater applications," *Materials Science in Semiconductor Processing*, vol. 127, no. pp. 105735, 2021.
- [67] Y.-R. Kim, J.-W. Park, S.-H. Park, and S.-J. Lee, "Radio-frequency and optically transparent radome de-icing materials: fluorine-doped tin oxide," *RSC Advances*, vol. 10, no. 59, pp. 35979-35987, 2020.